ISSN 1063-7729, Astronomy Reports, 2025, Vol. 69, No. 9, pp. 834–847. © Pleiades Publishing, Ltd., 2025.

Measurement of Radio Emission Scattering Parameters at the Frequency of 1650 MHz in the Direction of Pulsar B1937+21 with Ground–Space Interferometer RadioAstron

E. N. Fadeev[a],*, M. S. Burgin[a], M. V. Popov[a], A. G. Rudnitskiy[a], T. V. Smirnova[b], and V. A. Soglasnov[a]

[a]*Astrospace Center, Lebedev Physical Institute, Russian Academy of Sciences, Moscow, 117997 Russia*

[b]*Puschino Radio Astronomical Observatory, Astrospace Center, Lebedev Physical Institute, Russian Academy of Sciences, Puschino, Moscow oblast, 142290 Russia*

**e-mail: fadeev@asc.rssi.ru*

Received April 24, 2025; revised June 11, 2025; accepted June 27, 2025

Abstract—As part of the Early Science Program of the RadioAstron project, the millisecond pulsar B1937+21 was observed in October 2012. The total duration of the experiment supported by eight ground-based radio telescopes was about three hours. The radiation in both circular polarizations in the frequency band of 1644–1676 MHz was recorded. Characteristic time and frequency scales of scintillation caused by the scattering on the interstellar plasma density fluctuations have been measured: $\Delta t_{\rm dif} = 275.2 \pm 0.1$ s and $\Delta\nu_{\rm dif} = 580 \pm 30$ kHz. The angular diameter of the scattering disk, $\theta_{\rm H} = 0.32 \pm 0.03$ mas, has been estimated from the decrease in the amplitude of the interferometric response at the ground–space baselines. The dependence of the visibility amplitude on the delay shows two scattering time scales: $\tau_{\rm scl} = 110 \pm 30$ ns and $\tau_{\rm sc2} = 750 \pm 100$ ns, which indicates an ellipse-like scattering disc with an axis ratio of 2.6 : 1. The drift of the visibility maximum on the residual interference frequency that was observed at the intercontinental baselines can be explained by atmospheric effects, while the dominant contribution being the additional phase shift in the troposphere above European stations.

Keywords: interstellar plasma, radio pulsars, interstellar scintillation, VLBI

DOI: 10.1134/S1063772925702099

1. INTRODUCTION

In this paper, we continue the series of studies of the parameters of scattering of pulsar radio emission by inhomogeneities of interstellar plasma using the ground–space interferometer RadioAstron. Some of the results of these studies are discussed in [1–3] and the studies cited there.

Pulsar B1937+21 is located almost in the plane of the Galaxy (galactic coordinates: $l = 57°31'$, $b = -0°17'$). Astrometric VLBI observations have made it possible to estimate the distance to the pulsar as 2600^{+350}_{-290} pc and also module of $V_{\rm p} = 5 \pm 2$ km/s and the position angle of its tangential velocity vector of $(PA)_{\rm V} = 169.5° \pm 0.2°$ [4]. The dispersion measure measured in [5] is $DM = 71.1$ pc/cm^3.

B1937+21 is the first discovered millisecond pulsar [6]. Short pulse repetition period ($P \approx 1.557$ ms) and short pulse duration (≈150 μs) impose severe restrictions on the operation of the correlator; these restrictions will be discussed in Section 2. The average profile of the pulsar indicates the presence of an interpulse of the same duration as that of the main pulse, but with an amplitude that is half that of the main pulse [5].

Besides normal pulses, pulsar B1937+21 also emits so-called giant pulses [7, 8], which have a duration of less than 15 ns [9, 10]. In this paper, giant pulses are not studied, since due to their short duration, their analysis cannot be carried out using standard methods and requires the use of special algorithms that use coherent de-dispersion to compensate for the influence of interstellar dispersion on the characteristics of the received signal.

The observations used in this study were carried out within the framework of the Early Science Program of the RadioAstron project. In Section 2, the configuration of the ground-space radio interferometer used and the correlation processing method are described. Next, conclusions about the characteristics of the scattering medium made based on the analysis of the dynamic spectrum are provided (Section 3); the dependence of the interferometric visibility function

on various parameters is studied (Section 4); and conclusions are formulated (Section 5).

2. OBSERVATIONS AND CORRELATION DATA PROCESSING

The observations were carried out on October 22, 2012, and the total duration of the experiment was about three hours. The observations involved eight ground-based radio telescopes listed in Table 1.

The (u, v) plane coverage by the interferometer baselines during the experiment is illustrated in Fig. 1. These bases can be divided into three categories: small intra-European bases, intercontinental bases between Arecibo and European stations, and bases between ground-based radio telescopes and the RA. The longest ground-space baselines reached values of 27000 km, which provided a maximal angular resolution of ~1 mas.

The pulsar signal was recorded at the radio telescopes in a series of scans separated by 30-s intervals. The duration of the scans was 10 min for the last scan of the session and 9.5 min for the rest. Gain adjustment was performed by telescope operators, since the automatic gain control system was disabled. The entire experiment consisted of 18 scans with a total duration of approximately three hours. The measurements were made in two adjacent frequency subbands, each 16 MHz wide. The center frequency was set to 1660 MHz, so the total reception bandwidth was 1644–1676 MHz. All radio telescopes, except the Robledo observatory, recorded radio emission in two channels of circular polarizations (LCP and RCP). In Robledo, only left-hand polarization observations of the LCP were made.

The first step in obtaining information about the properties of the interstellar medium scattering the pulsar radiation from the observation results is preliminary processing, which includes correlation processing and normalization of the observational data. The purpose of preprocessing is to compute for each pair of antennas, hereinafter, designated a and b, dynamic cross-spectrum:

Table 1. List of telescopes

Telescope	Start of session	Duration, min
RA Radioastron	20:30:01	180
AR Arecibo	20:30:01	180
EF Effelsberg	20:30:01	180
JB Jodrell Bank	20:30:01	180
MC Medicina	20:30:07	159.9
NT Noto	20:30:01	169.5
RO Robledo	20:30:01	180
TR Torun	20:30:04	179.9
WB Westerbork	20:30:01	159.5

$$I_{ab}(\nu,t) = \langle \tilde{E}_a(\nu,t)\tilde{E}_b^*(\nu,t)\rangle, \quad (1)$$

which is a function of frequency ν and time t. Here, $\tilde{E}_a(\nu,t)$ and $\tilde{E}_b(\nu,t)$ denote the Fourier transforms of the electric field strengths of radiation received by antennas a and b, the superscript (*) is the complex conjugation, and $\langle\ldots\rangle$ is the averaging. In a particular case of $a = b$, the cross-spectrum is a real value and is proportional to the spectral flux density, and in the general case of $a \neq b$, is a complex quantity. Below, to shorten the notation, we will usually omit the indices indicating the used antennas.

Correlation processing was performed using the correlator of the LPI ASC [11]. To present information about the frequency dependence of $I(\nu,t)$, during correlation processing, the frequency band is divided into N_{ch} channels of equal width. Besides, when processing pulsar observations with the LPI ASC correla-

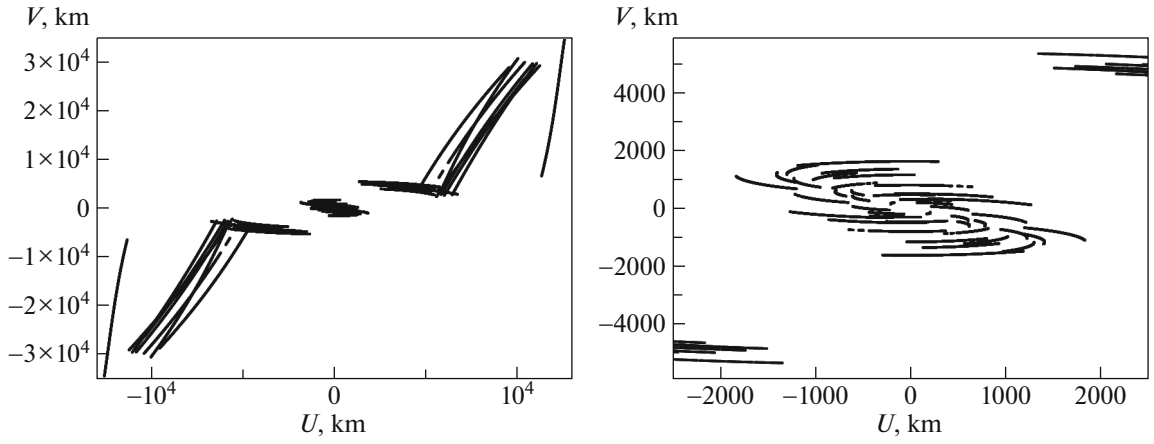

Fig. 1. The (u, v) coverage by the interferometer baselines. Left: All baselines. Right: A zoomed-in view of the central part, showing the intra-European baselines.

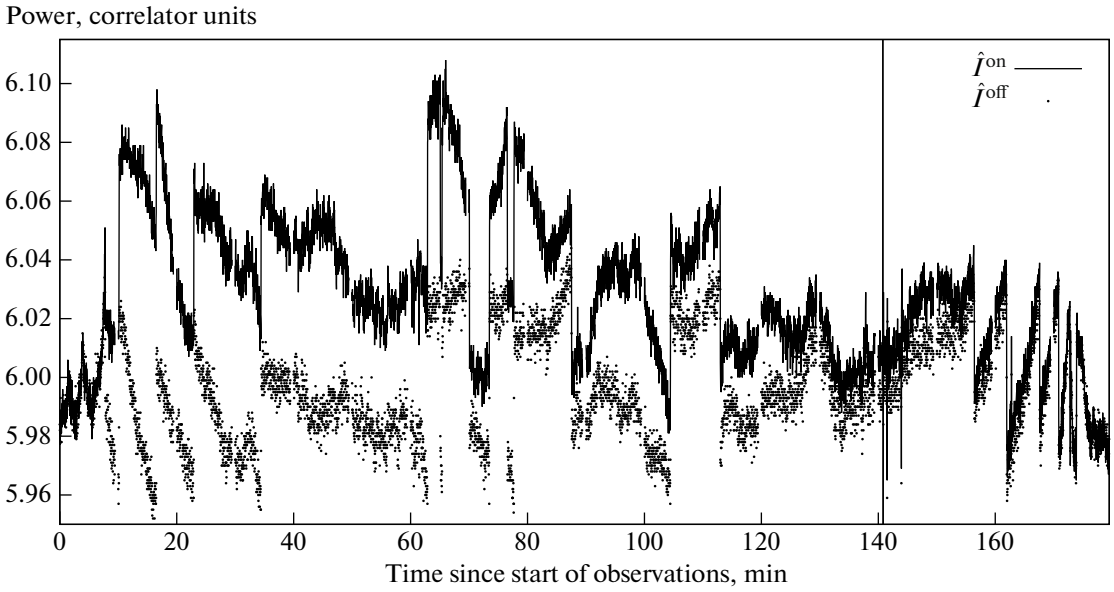

Fig. 2. Dependence of the registered power in the pulse ($\hat{I}^{on}$) and outside the pulse ($\hat{I}^{off}$) on the time for the antenna in Arecibo.

tor, correlation can be performed in arbitrarily specified "windows"—intervals that repeat with the pulsar period P. Typically, one of the windows used to measure the useful signal is selected to cover the main pulse, while one or two windows located in regions, where the pulsar emission is absent, are used to measure the noise of the system. A value of N_{ch} and the position of the correlation windows are user-defined parameters that determine the operating mode of the correlator and are selected based on the characteristics of the observed object and the scientific problems being solved.

The correlator selects data from files received from the interferometer stations in segments with a duration of $0.03125\ N_{ch}$ μs. The procedure for positioning the correlation window is carried out with an accuracy of up to the duration of these segments. To maximize increasing the signal-to-noise ratio, it is desirable that the positioning error be small compared to the duration of the main pulse, which for B1937+21 is 150 μs at a level of 0.1 of the maximal intensity. This condition determined the selection of the number of spectral channels of the correlator when processing each subband of $N_{ch}/2 = 128$, which corresponds to the positioning error of ≈8 μs and the frequency channel width of $\Delta\nu_{ch} = 125$ kHz.

For each pulsar period, uncalibrated cross-spectra were calculated in the pulse window ($\hat{I}^{on}$) and in the window outside the pulse ($\hat{I}^{off}$) for all interferometer baselines (see Fig. 2). Next, the results were averaged over intervals with a duration of $T_{av} = 1000P = 1.557$ s.

3. DYNAMIC SPECTRUM

We estimated the parameters characterizing the scattering of the pulsar's radio emission by the interstellar medium using a traditional analysis of dynamic auto-spectra. The initial data were the results of observations at Arecibo. The method we used for constructing dynamic spectra and calculating two-dimensional correlation functions from them is described in detail in the study of Fadeev et al. [1]. For clarity we will briefly summarize the key aspects of this method here.

The result of the dynamic auto-spectrum measurement obtained at the correlator output is a discrete sequence of instantaneous spectrum measurements, i.e., two-dimensional array $\hat{I}_{ij} = \hat{I}(\nu_i, t_j)$, which is a tabular function of frequency ν and time t. Here, $0 \le i < N_{ch}$ is the spectral channel index, while $0 \le j < N_p$ is the time-averaging interval index.

The signal measured in the on-pulse window contains both the pulsar radiation itself that is modified by the interstellar medium and receiver noise, as well as external interference. The off-pulse measurement allows the noise level to be estimated simultaneously with the signal recording. The response of the receiving system is not the same across the receiving band, but depends on the frequency in a complex way. During the session, the gain also does not remain constant. The signal increment in the on-pulse window is, to a first approximation, proportional to the system noise level. In this way, artificial distortions of the pulsar signal power arise in time and frequency within the

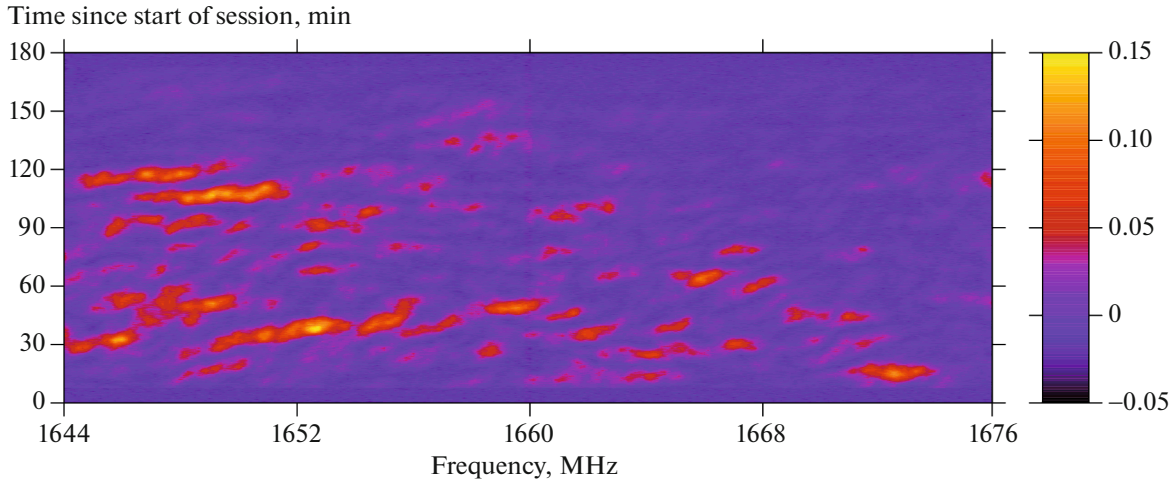

Fig. 3. Dynamic spectrum from Arecibo measurements that is summed over two polarization channels (LCP and RCP). The color scale on the right side of the figure establishes the correspondence between the color and the spectral flux density in the pulse that is normalized to the system noise.

dynamic spectrum. To correct for these distortions, we calculated the normalized dynamic spectrum:

$$I_{ij} = \frac{\hat{I}_{ij}^{\text{on}} - \langle \hat{I}_{ij}^{\text{off}} \rangle}{\langle \hat{I}_{ij}^{\text{off}} \rangle}. \quad (2)$$

Here, $\hat{I}_{ij}^{\text{on}}$ is the results of measurements in the on-pulse window, and $\langle \hat{I}_{ij}^{\text{off}} \rangle$ is the moving average of measurements in the off-pulse window.

The remaining significant interference in both subbands and both polarizations separately was replaced by random values with mean and variance determined in adjacent spectral regions, after which the spectra of the upper and lower subbands were combined, while the resulting spectra in the two polarizations were summed. Figure 3 shows the resulting dynamic spectrum.

As noted above, the signal was not detectable above the noise level in the first and last scans, but scintillation was clearly observed elsewhere. In the lower subband, the scintillation is expressed somewhat more pronounced than that in the upper one, although the noise level in both subbands is approximately the same.

To determine the scintillation characteristics, we calculated a two-dimensional correlation function:

$$DCCF(\Delta\nu_n, \Delta t_m) = \frac{\sum_{i=0}^{N_{\text{ch}}-1} \sum_{j=0}^{N_{\text{p}}-1} I_{ij} I_{i+n, j+m}}{(N_{\text{ch}} - n)(N_{\text{p}} - m)}, \quad (3)$$

where $\Delta\nu_n = n\Delta\nu_{\text{ch}} = 125n$ kHz,

$\Delta t_m = mT_{\text{av}} = 1.557m$ s (see Section 2),

$n = -N_{\text{ch}}/2 + 1, \ldots, N_{\text{ch}}/2 - 1$, and

$m = -N_{\text{p}}/2 + 1, \ldots, N_{\text{p}}/2 - 1$.

3.1. Scintillation Time and a Spectrum Index of Electron Density Fluctuations

The simplest quantitative characteristics describing the dependence of the dynamic spectrum on time and frequency that is caused by interstellar scintillations are the scintillation time Δt_{dif} and decorrelation bandwidth $\Delta\nu_{\text{dif}}$. To calculate these characteristics, time and frequency correlation functions, defined as $C_{\text{t}}(\Delta t_m) = DCCF(0, \Delta t_m)$ and $C_{\nu}(\Delta\nu_n) = DCCF(\Delta\nu_n, 0)$, are introduced, respectively. The scintillation time is defined as the half-width of the function $C_{\text{t}}(\Delta t_m)$ at the $1/e$ level of the maximum, while the scintillation bandwidth is the half-width at half maximum (HWHM) of $C_{\nu}(\Delta\nu_n)$.

One of the main parameters of the interstellar medium that influences the observed characteristics of scintillations is the shape of the spatial spectrum of electron density fluctuations. Information about the type of this spectrum is contained in the time structural function of the dynamic spectrum $S_{\text{t}}(\Delta t)$, which can be estimated from observations using the relation

$$S_{\text{t}}(\Delta t) = 2(C_{\text{t}}(0) - C_{\text{t}}(\Delta t)). \quad (4)$$

If the spectrum of fluctuations of the electron density of the interstellar plasma is described by a power law with exponent α_{e}, then according to [12],

$$\alpha_{\text{e}} = 2 + \left. \frac{d\left(\log S_{\text{t}}(\Delta t)\right)}{d\left(\log(\Delta t)\right)} \right|_{\Delta t \to 0}. \quad (5)$$

Basically, the values of Δt_{dif} and $\Delta\nu_{\text{dif}}$ can be found directly from experimentally obtained functions

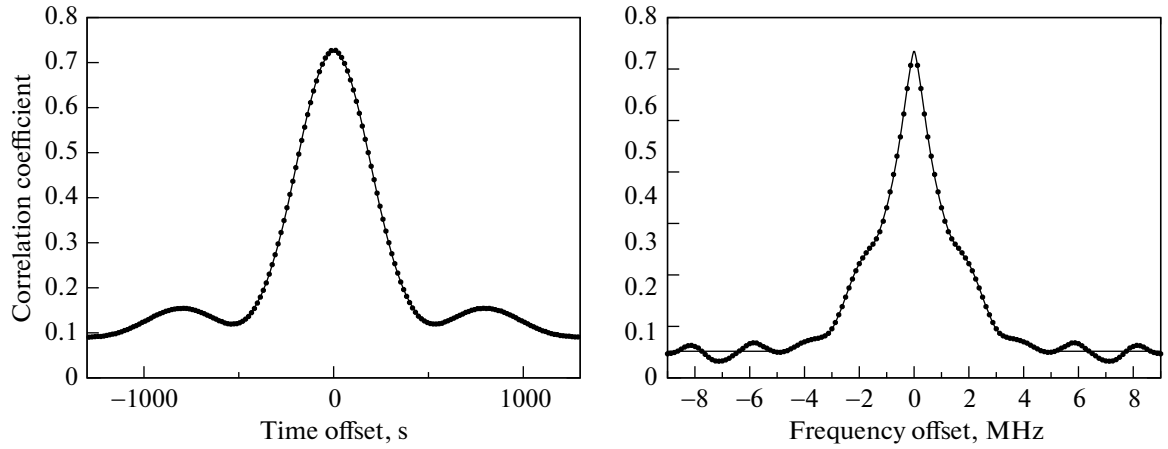

Fig. 4. Time (left) and frequency (right) autocorrelation functions. The data points obtained from the observations are shown as dots, and the best fit is shown as a solid line.

$C_t(\Delta t_m)$ and $C_\nu(\Delta\nu_n)$, and the value of α_e is by approximating the derivative in (5) by a finite difference. However, with this approach, the parameters are calculated based on only two or three measured values of the correlation functions, and due to the small number of data points used, instrumental noise has a strong influence on the final result. Furthermore, in the simplest method described above, one of the initial values is the $DCCF(0,0)$ value, which further increases the error of the result, since at the point (0,0), the influence of system noise is stronger than at other values of the arguments.

To improve accuracy, we adopted the following approach. Functions obtained from observations $C_t(\Delta t_m)$ and $C_\nu(\Delta\nu_n)$ were fitted with a priori specified analytical expressions by adjusting the free parameters included in these expressions. The fitting included all experimental points sufficiently close to zero, except for the zero point itself. Next, the calculation of the scintillation parameters was performed based on the obtained approximations. Thus, the measurement most susceptible to errors was completely excluded from consideration, while the random error of the sought parameters caused by noise was reduced by averaging over a large number of points considered in the fitting.

We used functions from the following family as approximators:

$$y(x\,|\,A,B,p,s,w) = A\exp(-(|x-s|/w)^p) + B, \quad (6)$$

where A, B, p, s, and w are free parameters as well as sums of these functions, if several scales were visible in the correlation function. This family was previously used in a similar situation in [1]. Values of $C_t(\Delta t_m)$ and $C_\nu(\Delta\nu_n)$, calculated from the observational results, along with the corresponding approximation fits, are illustrated in Fig. 4.

As can be seen from the figure, the function $C_t(\Delta t)$ is approximated very accurately by the sum of expressions from family (6) over a wide range of values Δt. The scintillation time value $\Delta t_{dif} \approx 275$ s obtained from this approximation agrees well with the conclusions of [13].

To determine α_e using (5), it is desirable to obtain as accurate an approximation as possible for $C_t(\Delta t)$ in the vicinity of the point $\Delta t = 0$. To eliminate the influence of measurements at large Δt on the calculation results when calculating α_e, the approximation by expression $y(\Delta t_m)$ with $s = 0$ on the interval of $\Delta t < \Delta t_{dif}/2$ was used, as a result, the value of $\alpha_e = 3.82 \pm 0.02$ was obtained.

Information about the spectrum of electron density fluctuations can also be extracted from the frequency dependence of the scattering time $\tau_{sc}(\nu)$. Namely, at a power-law spectrum of fluctuations with index α_e, the dependence of $\tau_{sc}(\nu)$ is described, according to [14], by a power-law with index α_{sc}, where $\alpha_e = 2\alpha_{sc}/(\alpha_{sc} - 2)$. Kondratiev et al. [15], based on their measurements at a frequency of 2100 MHz and on published data, determined the dependence of the scattering time on frequency for the pulsar B1937+21, $\tau_{sc} \propto \nu^{-4.2}$. This result corresponds to $\alpha_e = 3.82$, which coincides with the value we obtained.

Based on variations in the dispersion measure over a 20-year interval, Ramachandar et al. [16] obtained a value of $\alpha_e = 3.66 \pm 0.04$, which is close to the Kolmogorov value of $\alpha_e = 11/3$, for spatial scales corresponding to time shifts of 30–2000 days. Since, the time scales studied in that work are more than four orders of magnitude larger than those we studied, the difference between their results and ours can be inter-

preted as evidence for a dependence of the spectral index of inhomogeneities on the wavenumber.

3.2. Decorrelation Bandwidth

Sufficiently accurate approximation of the frequency autocorrelation function, $C_\nu(\Delta\nu)$, by the sum of expressions (6) turned out to be possible only at $\Delta\nu < 5$ MHz. The width of the decorrelation bandwidth is taken to be the width of the term with $s = 0$ at half maximum, which is equal to $\Delta\nu_{dif} = 580 \pm 30$ kHz.

The authors [13] approximated results of the measurement of C_ν at a frequency of $\nu = 1360$ MHz by the Lorentz function, ignoring the fact that the Lorentzian does not fit their data very well. Bringing the result they obtained of $\Delta\nu_{dif}(1360\ \text{MHz}) = 410$ kHz to our frequency using the scaling relation $\Delta\nu_{dif}(\nu) \propto \nu^{4.2}$ produces $\Delta\nu_{dif}(1660\ \text{MHz}) = 947$ kHz. It is difficult to identify unambiguously the main reason for the significant difference between the values obtained in [13] and in our study. The discrepancy may be due to the difference in methods used to determine $\Delta\nu_{dif}$. Furthermore, real variability in $\Delta\nu_{dif}$ can make a significant contribution: in [13], it is indicated that the values obtained from observations carried out on different days vary (after being converted to our frequency) between 846 and 1375 kHz.

In [17], relationships that connect the parameters of scattering screens and the "interstellar prism" with the structural function of the dynamic spectrum considered as a function of time, frequency, and coordinates of the observer were derived. In order to use the approach developed there, using a relation similar to (4), we calculated the frequency structure function $S_\nu(\Delta\nu)$ and tried to determine its behavior near the point $\Delta\nu = 0$ by a method similar to that used in analysis of the temporal structure function. In this case, we assumed that near zero, $S_\nu(\Delta\nu) \propto \Delta\nu^{-\alpha_\nu}$. However, the resulting value of $\alpha_\nu = 1.6$ (note that $\alpha_e = \alpha_\nu + 2$) is purely formal and cannot be used in the further analysis. The reason is the small number of experimental points satisfying the condition $\Delta\nu \ll \Delta\nu_{dif}$.

4. VISIBILITY FUNCTION

When constructing a radio image of the studied objects, the next step after obtaining the dynamic spectra, $I_{ab}(\nu,t)$, is usually the calculation of normalized interferometric visibility functions $V_{ab}(f_{res},\tau)$ as a function of the residual interference frequency, f_{res}, and delay, τ. The visibility function, $V_{ab}(f_{res},\tau)$, is, in essence, the cross-correlation coefficient of the electric fields of signals recorded at stations a and b at a time shift equal to τ. It is usually computed via a double Fourier transform of the dynamic cross-spectrum (an inverse transform in frequency, ν, and a forward transform in time, t), normalization of the amplitudes of signals received at stations, and a correction for system noise.

In an idealized situation of an observed object of simple structure, the use of precise ephemerides of the object, geometric parameters of the interferometer and clock corrections, a high signal-to-noise ratio, and the absence of noticeable distortions from the interstellar and interplanetary medium and the Earth's atmosphere in correlation processing, the amplitude of the visibility function, $|V_{ab}(f_{res},\tau)|$, is a unimodal function on the plane (f_{res},τ) with a maximum at $f_{res} = 0$, $\tau = 0$. A shift of the maximum away from this point contains information about the various parameters that characterize the difference between the real and idealized scenarios described above and about how these parameters evolve during the observation period.

4.1. Magnitude and Position of the Maximal Amplitude of the Visibility Function

One of the most important quantities obtained when processing interferometric observations is $|V|_{max}$, which is a value of $|V_{ab}(f_{res},\tau)|$ at the maximum. The value of $|V|_{max}$ carries information about the angular size of the observed object, and, in our case, about the extent of the scattering disk. Since the structure of the scattering disk can change during the observation period, and because various types of errors can shift the position of maximum of $|V|_{max}$ on the plane (f_{res},τ), the measurements should be divided into separate intervals, and the search for the maximum should be carried out independently for each interval.

From the point of view of reducing the error caused by random measurement errors, it is desirable to use the longest possible intervals. On the other hand, their duration is limited from above by the characteristic timescale of interstellar scintillations. As a compromise, we split each scan into two 285-s intervals, which is close to the value of $\Delta t_{dif} \approx 275$ s obtained in Section 3.

For each interval, an uncalibrated visibility function was calculated by Fourier transforming the initial dynamic spectrum, $\hat{V}_{ab}$, on a grid with steps in delay, τ, and interference frequency, f_{res}, that are equal to 31.25 ns and 3.5 MHz, respectively. In this case, only data from the lower subband (1644–1660 MHz), where the scintillation was more pronounced, were used (see Fig. 3).

The resulting value $\hat{V}_{ab}$ is expressed in the same units as the dynamic spectrum obtained by the correlator, i.e., in units of the signal recorders at the sta-

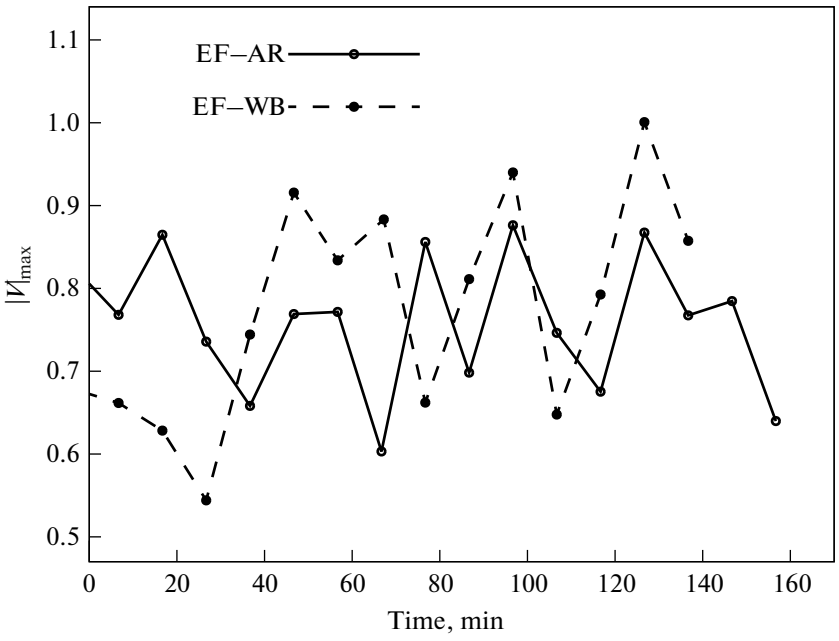

Fig. 5. Comparison of the amplitude of maxima of the normalized visibility function at the European (EF–WB) and intercontinental (EF–AR) interferometer baselines.

tions, and is distorted by the influence of system noise. Calculation of V_{ab} is produced using the ratio:

$$V_{ab} = \hat{V}_{ab}/R_{ab}\left(D_a^{\rm on}, D_a^{\rm off}, D_b^{\rm on}, D_b^{\rm off}\right), \qquad (7)$$

where $D_a^{\rm on}$ and $D_b^{\rm on}$ are the dispersions of the signals recorded at stations a and b, respectively, during the pulsar pulse, whereas $D_a^{\rm off}$ and $D_b^{\rm off}$ are the dispersions of signals outside the pulse.

For large ground-based radio telescopes (Arecibo, Effelsberg, and Westerbork), the difference $D^{\rm on} - D^{\rm off}$ is reliably estimated; the normalizing coefficient R in (7) was calculated using the formula:

$$R_{ab} = \sqrt{(D_a^{\rm on} - D_a^{\rm off})(D_b^{\rm on} - D_b^{\rm off})}. \qquad (8)$$

Normalization was carried out separately for two polarization channels. For further analysis, we used the values averaged over both channels.

The change over time of the maximal normalized amplitude of the visibility function at the Effelsberg–Westerbork (EF–WB) and Effelsberg–Arecibo (EF–AR) baselines is shown in Fig. 5. There is a significant variation in individual values. However, the average value of $|V|_{\rm max}$ is the same for both European and intercontinental baselines and amounts to 0.75 ± 0.05. The fact that a significant increase in the baseline projection does not lead to a decrease in $|V|_{\rm max}$ indicates that the scattering disk remains at the intercontinental baselines.

A significant deviation of the $|V|_{\rm max}$ value from unity for an unresolved source indicates that the normalizing coefficient, R, is calculated with a noticeable error. The reason for this is the significant non-stationarity of the system noise and the smallness of the $(D^{\rm on} - D^{\rm off})/D^{\rm off}$ value. Formula (8) is valid for a stationary noise signal. When applied to bright pulsars with periods of the order of a second, normalization was carried out for each individual pulse (see, for example, [18]), so that at each unit interval, the noise could be considered stationary with high accuracy.

In the case of the pulsar B1937+21, the determination of the visibility function was carried out over a time interval of 4.75 min that contained 1.8×10^5 individual pulses. Over such an interval, the non-stationarity of the noise becomes significant. In combination with the smallness of the signal increment in the pulse window over the noise outside the window, which even for the most sensitive radio telescope in Arecibo, does not exceed a few percent, and the variability of the signal due to scintillations, this leads to a bias in the estimate of R_{ab} and, consequently, $|V|_{\rm max}$.

Underestimation of the value $|V|_{\rm max}$ when calculating the normalizing coefficient using (8) at low values of the signal-to-noise ratio for an individual correlator output is illustrated in Fig. 6.

Another probable reason for the decrease in the amplitude of the visibility function is the influence of the Earth's atmosphere. detailed discussion is provided in Subsection 4.5.

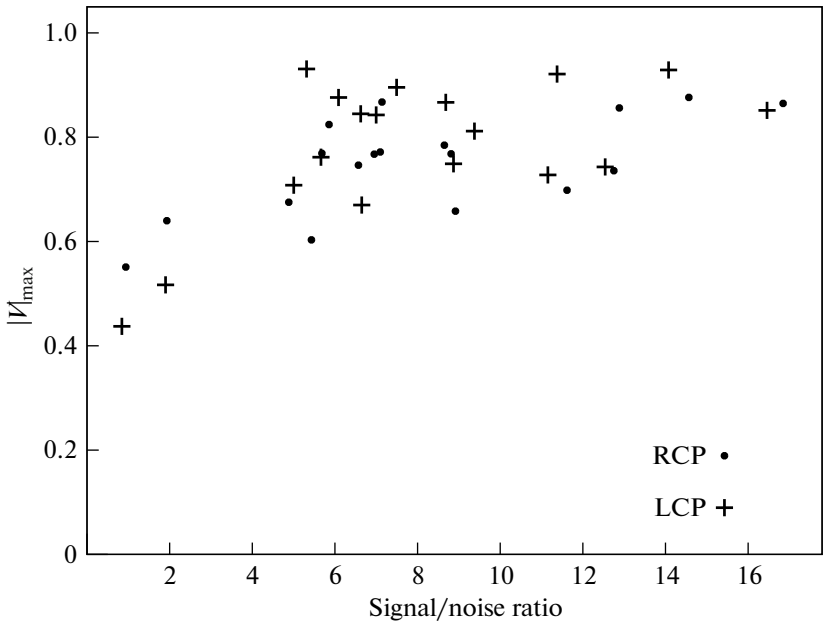

Fig. 6. Dependence of the maximum of the amplitude of the visibility function at the base (AR–EF) that is averaged over an interval of 4.75 min on the signal-to-noise ratio for an individual reading of the correlator.

Among the ground-space baselines, the interferometric signal was confidently detected at the RadioAstron-Arecibo (RA-AR) baseline only. On this basis, normalization of the visibility function using relation (8) is impossible, since the space radio telescope, unlike the ground-based ones, used single-bit quantization, resulting in $D_{RA}^{on} = D_{RA}^{off} \equiv 1$. Consequently, the method proposed by of Popov et al. [18] was applied to calculate the normalizing coefficient, leading to the following expression:

$$R = \left(D_{RA}^{off}/D_{AR}^{off}\right)^{1/2}\left(D_{AR}^{on} - D_{AR}^{off}\right)\sqrt{\eta}, \qquad (9)$$

where

$$\eta = 1.25 S_{RA}/S_{AR}. \qquad (10)$$

Here, S is the system's equivalent flux density, while the factor of 1.25 in (10) takes into account the difference in signal quantization methods on space (one-bit) and ground-based (two-bit) telescopes.

Figure 7 shows the dependence of the visibility amplitude on the projected baseline length of the ground-space interferometer. The average value of $|V|_{max}$ was 0.86 ± 0.05, which is somewhat higher than the average value on the ground-based baselines (0.75 ± 0.05). This can be understood if we attribute the decrease in the amplitude of the visibility function on the ground-based baselines to the influence of the atmosphere on the results of measurements at European telescopes, since the space telescope is located outside the atmosphere, and the Arecibo radio telescope observed in directions close to the zenith.

In Fig. 7, one can also notice a tendency towards a decrease in the amplitude of the visibility function with an increase in the baseline length of the ground-space interferometer. We attempted to estimate the size of the scattering disk using these data. The solid line represents the fit of the observational data to a scattering disk model with a width of $\theta_H = 0.32 \pm 0.03$ mas. For the fit, we used the dependence of the amplitude of the visibility function, $|V|_{max}(B)$, on the projected baseline length, B:

$$|V|_{max}(B) = \exp\left[-\frac{1}{2}\left(\frac{\pi}{\sqrt{2\ln 2}}\frac{\theta_H B}{\lambda}\right)^{\alpha_e - 2}\right], \qquad (11)$$

from the study of Gwinn et al. [19]. Here, λ is the observation wavelength, θ_H is the full width at half maximum (FWHM) diameter of the pulsar's scattered image disk, and $\alpha_e = 3.82$ is the exponent of the spatial spectrum of electron density fluctuations (see Section 3).

4.2. Determination of the Scattering Time from the Dependence of the Visibility Function on the Delay

Information about the geometry of the scattering disk is contained in the dependence of $|V(f_{res}, \tau)|$ on delay τ at a fixed $f_{res} = f_m$. Here, f_m is the value of f_{res}, at which the maximum of $|V|$ is achieved. To analyze the dependence $|V(f_{res}, \tau)|$, we selected scans on the EF–AR baseline for which the condition

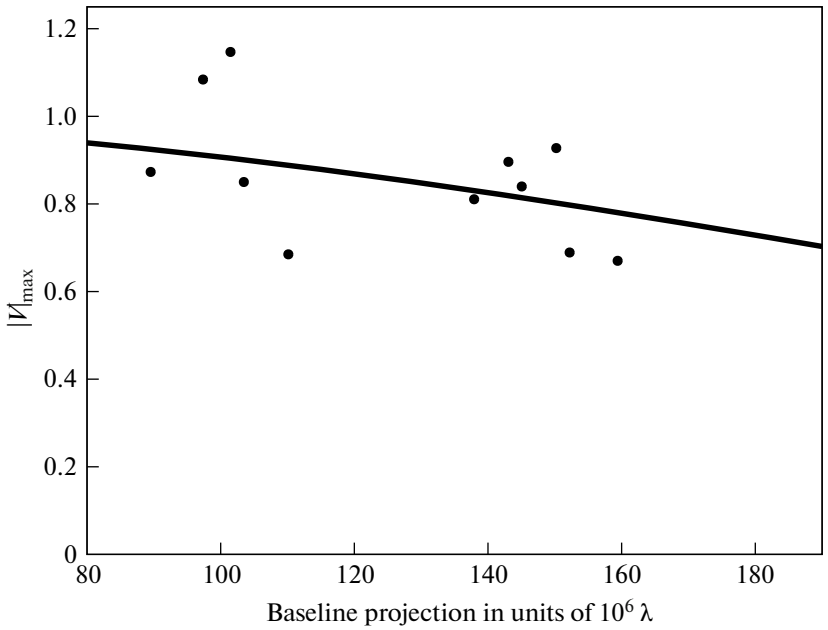

Fig. 7. Dependence of the maximum of the amplitude of the visibility function on the projected baseline length (RA–AR). The solid line shows the approximation of the data by the model of a scattering disk with a radius of 0.3 mas.

$|V|_{max} > 10\sigma_V$ was satisfied, where σ_V is the root-mean-square (rms) error $|V|$. For all these scans, the value of f_m turned out to be equal to zero, while the τ values, for which $|V|$ reaches its maximum, are the same. For further comparison with the theoretical model, the function $|V|_a(\tau)$ which is average value for the selected scans $|V(0,\tau)|$, was used.

When interpreting observational data, the influence exerted on the measurement results of $|V|_a(\tau)$ by fluctuations in the intensity of radiation generated by the pulsar with characteristic times comparable to and shorter than the accumulation time of the interferometric signal should be taken into account. In Rickett's study [20], the autocorrelation function of the recorded signal in the so-called amplitude-modulated noise approximation was calculated. In this approximation, the pulsar's radiation intensity is approximated by the product of white noise and a function describing the pulsar's average pulse profile. In this case, the autocorrelation function of the recorded signal is represented as the sum of two components: a narrow noise peak near the delay of $\tau = 0$ and a relatively slowly changing pedestal carrying information about the pulse shape.

The noise peak arises as a consequence of the fact that the autocorrelation function of white noise is the Dirac δ-function. For the observed signal, the peak amplitude is finite, while the width is non-zero due to smoothing of the input noise by the recording system with a finite bandwidth.

As noted above, the visibility function calculated during the processing of VLBI observations is the cross-correlation function of the signals recorded at the baseline antennas. The intensity of the radiation generated by the pulsar enters as a multiplier into the signal recorded by both antennas. Due to this, the influence of the noise nature of the pulsar radiation on the statistical characteristics of the measured visibility function near $\tau = 0$ is very similar to what occurs in single-antenna observations. In this case, the parameters of the noise peak depend mainly not on the characteristics of the scattering medium, but on the properties of the pulsar itself and the parameters of the interferometer. In particular, the bandwidth of the receiver–correlator system and, therefore, the width of the noise peak are determined by the signal accumulation time during correlation. In our case, the noise peak includes three points: the point at $\tau = 0$ and two adjacent to it.

In the study by Popov et al. [21], based on observations of five pulsars performed using a ground–space interferometer, the fine structure of the function (in our notation) $|V|_a(\tau)$ near $\tau = 0$ was analyzed. As in our case, the measurement results were well described by the amplitude-modulated noise model and could be represented as the sum of two components with approximately equal values at $\tau = 0$: narrow noise peak near $\tau = 0$ and a smooth function that decreases slowly with increasing $|\tau|$.

When comparing observational data with the results of model calculations, an approach similar to that used in [21] was used in our study. Since informa-

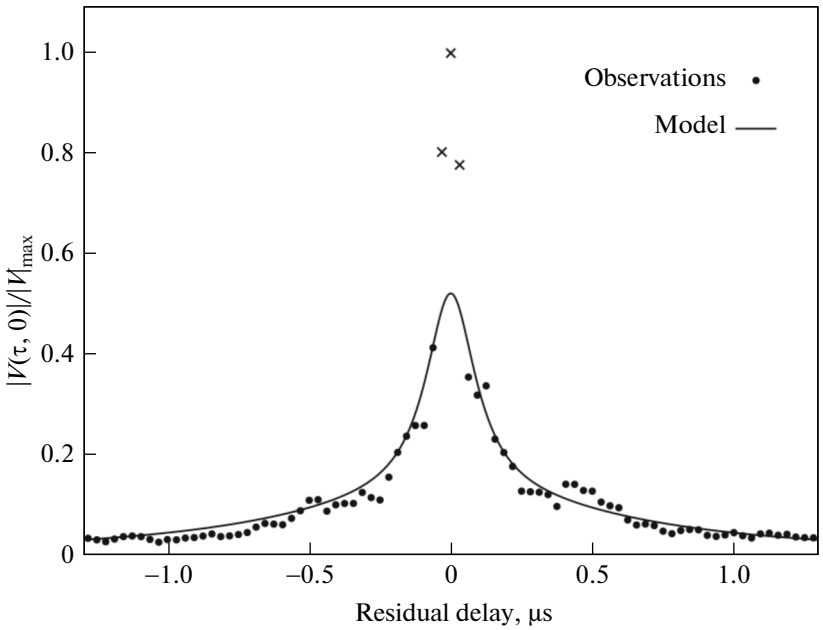

Fig. 8. Observed and model dependences of the amplitude of the normalized visibility function on the residual delay at the base (EF–AR). Results of measurements near $\tau = 0$, marked with the symbol "×", are distorted by the noise signal of the pulsar and were not taken into account when determining the parameters of the model. The sum of two Lorentz functions with half-widths of $\tau_{sc1} = 0.11 \pm 0.03$ μs, $\tau_{sc2} = 0.75 \pm 0.01$ μs was used as a model approximation.

tion about the structure of the scattering disk is contained in the broad component, measurements at those τ values, in which the contribution of the noise peak is noticeable, were not taken into account in the analysis. Measured values of $|V|_a(\tau)$ and the model function approximating them are shown in Fig. 8.

The characteristics of the scattering disk are determined by fitting the broad component with a theoretical model. In the simplest case of a circular scattering disk formed on a thin phase screen, the model dependence of the broad component has the form:

$$|V|_a(\tau) = |V|^{(w)}_{max} L(\tau, \tau_{sc}), \quad (12)$$

where $|V|^{(w)}_{max}$ is the amplitude of the broad component, and the Lorentz function, L, is given by the expression:

$$L(\tau, \tau_{sc}) = \frac{\tau^2_{sc}}{\tau^2 + \tau^2_{sc}}, \quad (13)$$

while the scattering time τ_{sc} is determined by the angular size of the scattering disk and the distances of the screen and the pulsar from the observer.

In our case, it was not possible to find a satisfactory approximation of the measurement results using model (12), and for the approximation $|V|(\tau)$, we used the sum of two terms (12). As can be seen from Fig. 8, this model with $\tau_{sc1} = 0.11 \pm 0.03$ μs and $\tau_{sc2} = 0.75 \pm 0.01$ μs is a good approximation to the observed broad component. According to [21, 22], two essentially different time scales arise in the dependence of $|V|_a(\tau)$ in the case, where the scattering disk has an elliptical shape. Following the approach outlined in these studies, we obtain that since $\tau_{sc} \propto \theta^2_H$, then the major and minor axes of the scattering disk are related as 2.6 : 1.

In [16], variations of τ_{sc} over time (1996–2004) in the range from 90 to 155 μs were observed at a frequency of 327 MHz. Based on the average value of $\tau_{sc} = 120$ μs and the frequency dependence of $\tau_{sc}(\nu) \propto \nu^{-4.4}$, we obtain $\tau_{sc} = 0.094$ μs at 1660 MHz, which is in good agreement with our measured value of 0.11 μs.

4.3. Analysis of Secondary Spectra

The secondary spectrum is the square of the result of the two-dimensional Fourier transform of the dynamic spectrum, $|\tilde{I}(\tau, f_{res})|^2 = |\mathcal{F}_2[I(\nu, t)]|^2$. Steinbring et al. [23] found that the secondary spectra of a number of pulsars contain specific structures called parabolic arcs. They arise due to interference of the pulsar's radiation on individual elements of the substructure within the pulsar's scattering disk. It has been shown [24, 25] that a strong elongation of the scattering disk is one of the necessary conditions for the formation of parabolic arcs. The asymmetry of the scattering disk that we found is consistent with this condition for the appearance of arcs.

We constructed the secondary spectrum from the dynamic spectrum obtained at Arecibo and found no traces of parabolic arcs. Turner et al. [13], who con-

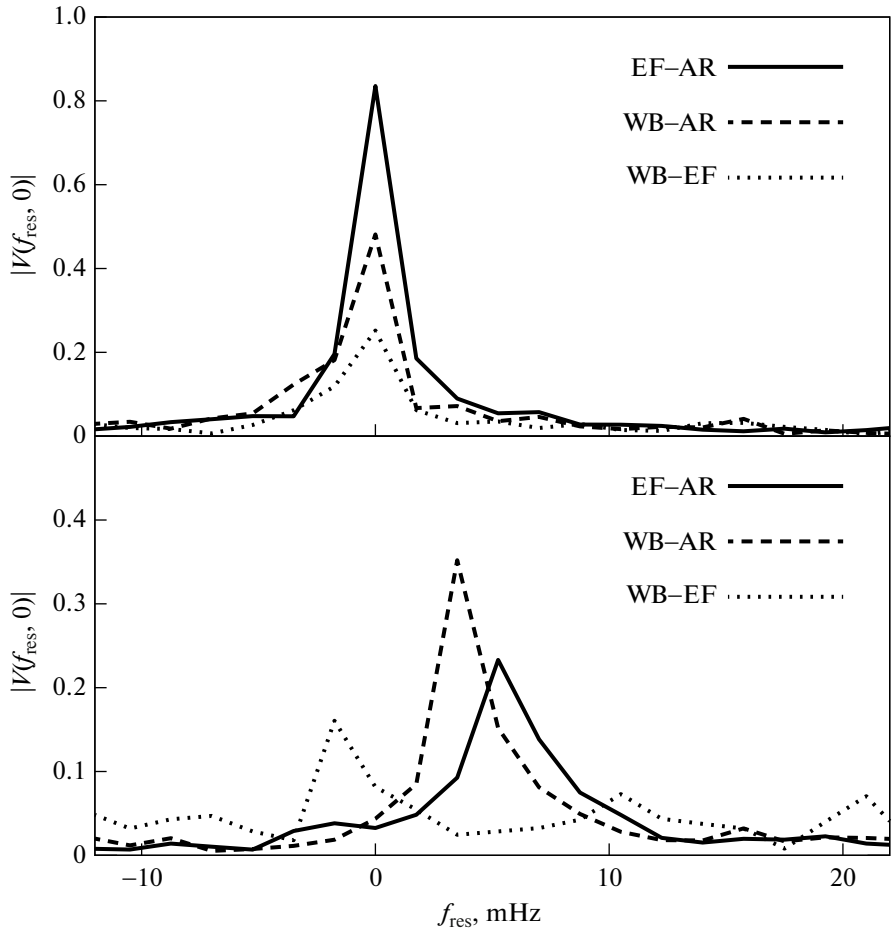

Fig. 9. Visibility amplitude as a function of the residual interference frequency. The top panel corresponds to the beginning of the observation session (T = 21 h), and the bottom panel corresponds to the end (T = 23 h).

ducted observations with the Arecibo telescope a month earlier, detected two parabolic arcs in the secondary spectrum of the pulsar B1937+21. They showed that the arc contrast decreases drastically with increasing frequency from 1285 to 1460 MHz. Our observations were at 1660 MHz with a comparable receiver bandwidth, and, therefore, the absence of arcs in our data is consistent with the found trend.

4.4. Displacement of Maximum of $|V|$ in Residual Interference Frequency

The difference f_m (the residual interference frequency, at which the maximum visibility amplitude is achieved) from zero and the change in f_m during the observation period are a sensitive indicator of the impact of various factors that distort the correlation results. To estimate the influence of these factors on the final results, calculations of $|V(f_{res}, 0)|$ were carried out separately for each scan lasting 570 s, which provided resolution in an interference frequency of 1.75 mHz.

The dependence of the function $|V(f_{res}, 0)|$ on the residual interference frequency at the beginning and end of the observations is shown in Fig. 9. At the intercontinental baselines EF–AR and WB–AR, a shift in the maximum by ≈8 mHz is observed during the observation session, while on the short EF-WB baseline, such a shift is absent. The width of the maximum of the function $|V(f_{res}, 0)|$ measured at half-width at half-maximum varies from 1 to 3 mHz. Possible reasons for these variations in the shape and position of the maximum of $|V(f_{res}, 0)|$ will be discussed in Subsection 4.5.

4.5. Distortion of the Interferometric Signal by the Earth's Atmosphere

One of the sources of errors in the results of measurements of the parameters of the scattering disk are distortions introduced by the Earth's atmosphere. Theoretical models explaining the origin of these distortions and making it possible to estimate their impact on the observation results are described in [26]

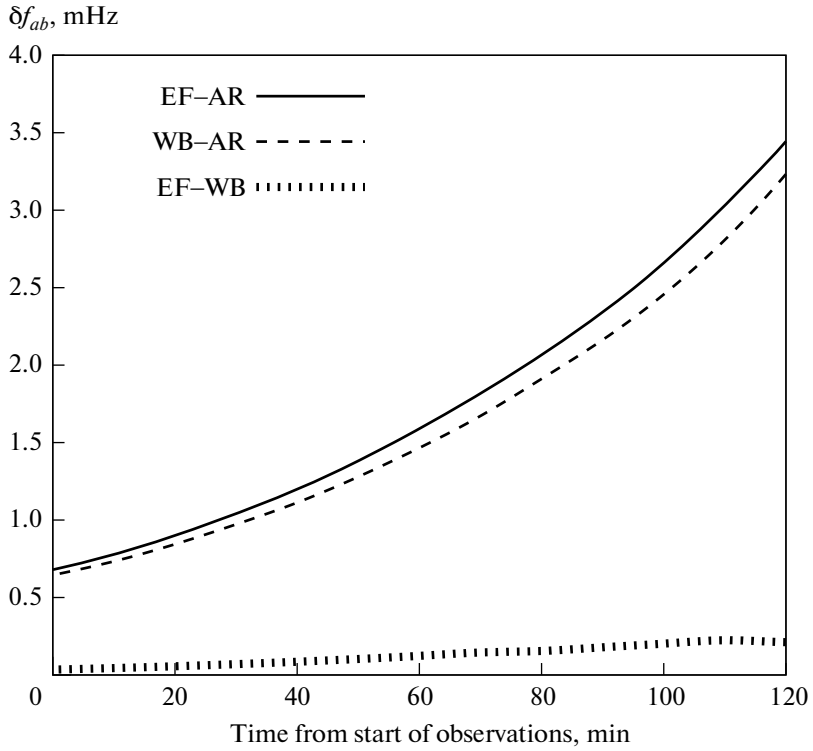

Fig. 10. Atmospheric-induced variations in the residual interference frequency on an intercontinental and intra-European baselines.

and the references therein. A quantitative characteristic of atmospheric effects influencing the results of VLBI observations is $L(t)$, atmospheric-induced change in the optical path along the line of sight. Atmospheric distortions of the optical path cause a phase shift of the signal received at the station by $\varphi = 2\pi L/\lambda$, where $\lambda = 18$ cm is the wavelength, and the phase shift of the cross-spectrum for the baseline $a - b$ by $\Delta\varphi_{ab} = \varphi_a - \varphi_b$. The variability of atmospheric distortions leads to a shift in the residual interference frequency by

$$\delta f_{ab} = \frac{d\Delta\varphi_{ab}}{dt}. \quad (14)$$

Accurate calculation of the dependence of $L(t)$ on time t for each of the ground stations participating in the observations requires taking into account both the change in zenith distance $z(t)$ of the observed object during the session and variations in the atmospheric parameters above the station. As was noted above (see Fig. 9), on long baselines between Arecibo and the European stations, the shift of the maximum of the function $|V_{ab}(f_{\text{res}}, \tau)|$ by f_{res} during the session exceeds significantly the shift for relatively short baselines between European stations. This difference is naturally explained if the dominant cause of variability in $L(t)$ is a change in zenith distance. For the Arecibo–Europe baselines, the zenith distances of the source at the stations vary greatly and change differently during the observation period, while for the European stations, which are close to each other, the zenith distances remain close to each other all the time.

The source's zenith distance at Arecibo did not exceed 20° during the entire session, whereas at the European stations, observations were carried out at larger and increasing zenith distances towards the end of the session. In particular, at the moment of completion of observations in Westerbork at 23:09:30 UTC, the zenith distance in Effelsberg and Westerbork was 72.6° and 71.9°, respectively. Since the phase distortion of the cross-spectra at the correlator output is determined by the difference between the $L(t)$ values for each pair of stations, and the $L(t)$ value, especially its tropospheric component, increases significantly as the line of sight approaches the horizon, then at intercontinental baselines, the dominant factor is the additional phase shift in the troposphere above European stations.

An estimate shown below of the contribution of the atmosphere to the results of cross-spectrum measurements is based on static models of the troposphere and ionosphere, for which the dependencies of $L(z)$ are given in [26]. An atmospheric shift of the residual interference frequency for the baseline $a - b$ was calculated using the relationship:

$$\delta f_{ab} = \frac{1}{\lambda}\left(\frac{dL_a(z)}{dz}\frac{dz_a(t)}{dt} - \frac{dL_b(z)}{dz}\frac{dz_b(t)}{dt}\right), \quad (15)$$

and the calculation results are illustrated in Fig. 10.

The obtained theoretical estimate of the atmospheric shift of the residual interference frequency of ≈3 MHz during observations at intercontinental baselines is a little less than the value of ≈5 MHz obtained from measurements. However, it should be noted that the atmospheric model used for the estimate is a very rough approximation of reality. The main sources of error are the static nature of the troposphere model and the lack of consideration of the influence of water vapor. Therefore, atmospheric influence appears to be the most likely cause of the observed shift.

In the static model of the Earth's atmosphere used above, variations in phase disturbances are associated only with changes in the zenith distance of the pulsar. Therefore, the shift that arises as a consequence of these disturbances in f_m becomes noticeable only at relatively large time intervals exceeding the duration of the scan (10 min). Variations in f_m with shorter characteristic times can be caused by non-stationary processes in the atmosphere. The most likely cause of these rapid variations in our case is the variability of the column density of water vapor, which can be especially strong during observations at large zenith distances, i.e., at European stations toward the end of the session.

Variability in f_m with a characteristic time less than the accumulation time used in calculating the function $|V(f_{res}, \tau)|$ leads to the fact that the peak of $|V|$ considered as a function of the argument f_{res} becomes wider, while $|V|_{max}$, a value of $|V|$ at maximum, decreases. In Fig. 9, it is shown that this is exactly the situation observed in our measurements.

5. CONCLUSIONS

Using a ground-space radio interferometer, observations of the ms pulsar B1937+21 were carried out at a frequency of 1660 MHz with baseline projections of up to 27000 km. Using dynamic spectrum analysis techniques, we studied the characteristics of interstellar scintillations. Based on the analysis of data obtained at the Arecibo radio telescope, the largest of the ground-based telescopes participating in the experiment, the values obtained for the scintillation time and decorrelation bandwidth were, respectively, $\Delta t_{dif} = 275.2 \pm 0.1$ s and $\Delta\nu_{dif} = 580 \pm 30$ kHz.

Using the relation between the time structural function of interstellar scintillations and statistical characteristics of electron density fluctuations in the scattering plasma, an estimate of $\alpha_e = 3.82 \pm 0.02$ was obtained for the index of the power spectrum of these fluctuations. This estimate coincides with the result presented in [15] and obtained based on studying the frequency dependence of the scattering time. Comparison of our value with the results of [16] suggests a dependence of α_e on the wave number.

The interferometric response was detected both at ground-based baselines and at the Arecibo–RadioAstron baseline. Comparison of $|V|_{max}$, the maximum amplitude of the visibility function, at relatively small intra-European bases and at the intercontinental Arecibo–Europe baselines shows that even at the longest ground-based baselines, the scattering disk is not resolved. The dependence of $|V|_{max}$ on time exhibits strong random fluctuations (see Figs. 5 and 6). For the average value of this quantity, we obtained $\langle|V|_{max}\rangle \approx 0.75$, which is significantly lower than the value $\langle|V|_{max}\rangle = 1$ that is expected for an unresolved source. This decrease in the average level and strong fluctuations are due to two reasons. First, the mentioned effects can be caused by atmospheric distortions. Second, the method used to calculate the visibility function leads to a biased estimate of $|V|_{max}$ due to the small and highly non-stationary signal-to-noise ratio of the initial measurements at the interferometer stations.

On the AR–RA ground-space baseline, a decrease in $\langle|V|_{max}\rangle$ with increasing projected baseline length is observed. A comparison of measurements with the theoretical model yields an estimate of $\theta_H = 0.32 \pm 0.05$ mas for the angular size of the cross-section of the scattering disk along the baseline direction.

The dependence of the amplitude of the visibility function on the delay (Fig. 8) indicates the presence of two characteristic scattering times: $\tau_{sc1} = 0.11 \pm 0.03$ μs and $\tau_{sc2} = 0.75 \pm 0.01$ μs. This indicates that the shape of the scattering disk is close to an ellipse with an axial ratio of 2.6 : 1.

On intercontinental baselines, a systematic shift in the position of the maximum of the visibility function in the interference frequency is observed. This shift is shown to be caused mainly by distortions arising in the troposphere. The largest contribution comes from distortions at European stations, where observations were carried out at large zenith angles. The shift of the visibility function in interference frequency on long baselines may also be partly due to the effect of refraction on inhomogeneities in the interstellar plasma.

ACKNOWLEDGMENTS

The RadioAstron project was led at the Astrospace Center of the Lebedev Physics Institute, Russian Academy of Sciences. and the Lavochkin Scientific and Production Association under a contract with the State Space Corporation ROSCOSMOS together in collaboration with partner organizations in Russia and other countries.

FUNDING

This work was supported by ongoing institutional funding. No additional grants to carry out or direct this particular research were obtained.

CONFLICT OF INTEREST

The authors of this work declare that they has no conflicts of interest.

REFERENCES

1. E. N. Fadeev, A. S. Andrianov, M. S. Burgin, M. V. Popov, A. G. Rudnitskiy, T. V. Smirnova, and V. A. Soglasnov, Astron. Rep. **68**, 1076 (2024).
2. M. V. Popov, N. Bartel, A. S. Andrianov, M. S. Burgin, et al., Astrophys. J. **954**, 126 (2023).
3. M. V. Popov and T. V. Smirnova, Astron. Rep. **65**, 1129 (2021).
4. H. Ding, A. T. Deller, B. W. Stappers, T. J. W. Lazio, et al., Mon. Not. R. Astron. Soc. **519**, 4982 (2023).
5. V. M. Kaspi, J. H. Taylor, and M. F. Ryba, Astrophys. J. **428**, 713 (1994).
6. D. C. Backer, S. R. Kulkarni, C. Heiles, M. M. Davis, and W. M. Goss, Nature (London, U.K.) **300** (5893), 615 (1982).
7. A. Kinkhabwala and S. E. Thorsett, Astrophys. J. **535**, 365 (2000).
8. J. W. McKee, B. W. Stappers, C. G. Bassa, S. Chen, et al., Mon. Not. R. Astron. Soc. **483**, 4784 (2019).
9. V. A. Soglasnov, M. V. Popov, N. Bartel, W. Cannon, A. Yu. Novikov, V. I. Kondratiev, and V. I. Altunin, Astrophys. J. **616**, 439 (2004).
10. V. I. Kondratiev, M. V. Popov, V. A. Soglasnov, Y. Y. Kovalev, N. Bartel, and F. Ghigo, in *Proceedings of the WE-Heraeus Seminar on Neutron Stars and Pulsars 40 years after the Discovery,* Ed. by W. Becker and H. H. Huang (2007), p. 76.
11. S. F. Likhachev, V. I. Kostenko, I. A. Girin, A. S. Andrianov, A. G. Rudnitskiy, and V. E. Zharov, J. Astron. Instrum. **6**, 1750004-131 (2017).
12. V. I. Shishov, T. V. Smirnova, W. Sieber, V. M. Malofeev, et al., Astron. Astrophys. **404**, 557 (2003).
13. J. E. Turner, T. Dolch, J. M. Cordes, S. K. Ocker, et al., Astrophys. J. **972**, 16 (2024).
14. R. W. Romani, R. Narayan, and R. Blandford, Mon. Not. R. Astron. Soc. **220**, 19 (1986).
15. V. I. Kondratiev, M. V. Popov, V. A. Soglasnov, Y. Y. Kovalev, N. Bartel, W. Cannon, and A. Yu. Novikov, Astron. Astrophys. Trans. **26**, 585 (2007).
16. R. Ramachandran, P. Demorest, D. C. Backer, I. Cognard, and A. Lommen, Astrophys. J. **645**, 303 (2006).
17. T. V. Smirnova, V. I. Shishov, M. V. Popov, C. R. Gwinn, et al., Astrophys. J. **786**, 115 (2014).
18. M. V. Popov, N. Bartel, C. R. Gwinn, M. D. Johnson, et al., Mon. Not. R. Astron. Soc. **465**, 978 (2017).
19. C. R. Gwinn, J. M. Cordes, N. Bartel, A. Wolszczan, and R. L. Mutel, Astrophys. J. Lett. **334**, L13 (1988).
20. B. J. Rickett, Astrophys. J. **197**, 185 (1975).
21. M. V. Popov, N. Bartel, M. S. Burgin, C. R. Gwinn, T. V. Smirnova, and V. A. Soglasnov, Astrophys. J. **888**, 57 (2020).
22. C. R. Gwinn, M. V. Popov, N. Bartel, A. S. Andrianov, et al., Astrophys. J. **822**, 96 (2016).
23. D. R. Stinebring, M. A. McLaughlin, J. M. Cordes, K. M. Becker, J. E. Espinoza Goodman, M. A. Kramer, J. L. Sheckard, and C. T. Smith, Astrophys. J. Lett. **549**, L97 (2001).
24. M. A. Walker, D. B. Melrose, D. R. Stinebring, and C. M. Zhang, Mon. Not. R. Astron. Soc. **354**, 43 (2004).
25. J. M. Cordes, B. J. Rickett, D. R. Stinebring, and W. A. Coles, Astrophys. J. **637**, 346 (2006).
26. A. R. Thompson, J. M. Moran, and G. W. Swenson, Jr., *Interferometry and Synthesis in Radio Astronomy,* 3rd ed. (Springer, Cham, 2017).